Remote Sensing and Modeling of Coherent Structures in River and Estuarine Flows

Andrew T. Jessup
Applied Physics Laboratory
University of Washington
Seattle, WA 98195-5640
phone: (206) 685-2609 fax: (206) 543-6785 email: jessup@apl.washington.edu

Robert L. Street
Department of Civil and Environmental Engineering
Stanford University, Stanford, CA 94305-4020
phone: (650) 723-4969 fax: (650) 725-39720 e-mail: street@stanford.edu

Stephen G. Monismith
Department of Civil and Environmental Engineering
Stanford University, Stanford, CA 94305-4020
phone: (650) 723-4764 fax: (650) 725-9720 email: monismith@stanford.edu

Alexander R. Horner-Devine
Department of Civil and Environmental Engineering
University of Washington
Seattle, WA 98195-2700
Phone: (206) 685-3032 fax: (206) 685-9185 email: arhd@u.washington.edu

Award Numbers: N00014-05-1-0485 (MURI), N00014-07-1-0898 (DURIP)

LONG-TERM GOALS

The long-term goals of this research are to combine state-of-the-art remote sensing and *in situ* measurements with advanced numerical modeling (a) to characterize coherent structures in river and estuarine flows and (b) to determine the extent to which their remotely sensed signatures can be used to initialize and guide predictive models.

OBJECTIVES

Coherent structures are generated by the interaction of the flow with bathymetric and coastline features. These coherent structures produce surface signatures that can be detected and quantified using remote sensing techniques. Furthermore, a number of relationships between coherent structures and flow characteristics have been suggested that have the potential to allow flow parameters (e.g. mean velocity, bottom roughness, shear, and turbidity) to be inferred from remote measurements. The objectives are to test the following four hypotheses:

1. Flow parameters can be inferred from remotely sensed signatures of coherent structures.
2. Numerical models can be constrained with these inferred parameters.

Report Documentation Page

Form Approved
OMB No. 0704-0188

1. REPORT DATE	2. REPORT TYPE	3. DATES COVERED
30 SEP 2008	**Annual**	**00-00-2008 to 00-00-2008**

4. TITLE AND SUBTITLE	5a. CONTRACT NUMBER
Remote Sensing And Modeling Of Coherent Structures In River And Estuarine Flows	5b. GRANT NUMBER
	5c. PROGRAM ELEMENT NUMBER
6. AUTHOR(S)	5d. PROJECT NUMBER
	5e. TASK NUMBER
	5f. WORK UNIT NUMBER
7. PERFORMING ORGANIZATION NAME(S) AND ADDRESS(ES) **University of Washington ,Applied Physics Laboratory,Seattle,WA,98195-5640**	8. PERFORMING ORGANIZATION REPORT NUMBER
9. SPONSORING/MONITORING AGENCY NAME(S) AND ADDRESS(ES)	10. SPONSOR/MONITOR'S ACRONYM(S)
	11. SPONSOR/MONITOR'S REPORT NUMBER(S)

12. DISTRIBUTION/AVAILABILITY STATEMENT
Approved for public release; distribution unlimited

13. SUPPLEMENTARY NOTES

14. ABSTRACT
The long-term goals of this research are to combine state-of-the-art remote sensing and in situ measurements with advanced numerical modeling (a) to characterize coherent structures in river and estuarine flows and (b) to determine the extent to which their remotely sensed signatures can be used to initialize and guide predictive models.

15. SUBJECT TERMS

16. SECURITY CLASSIFICATION OF:			17. LIMITATION OF ABSTRACT	18. NUMBER OF PAGES	19a. NAME OF RESPONSIBLE PERSON
a. REPORT	b. ABSTRACT	c. THIS PAGE			
unclassified	**unclassified**	**unclassified**	**Same as Report (SAR)**	**22**	

3. The effect of stratification on the strength of coherent structures can be used to detect the presence or absence of stratification and the location of the fresh/salt water interface.
4. Numerical and field experiments can be used together to predict, interpret, characterize, and understand coherent structures.

APPROACH

The key to this project is an interactive process that blends sophisticated remote sensing, in-situ measurements, and numerical simulation. Our approach is to conduct closely coupled field and numerical model experiments to test the hypotheses listed above. The plan includes two major field experiments with both *in situ* and remote sensing measurements – the first occurred in 2006 (Year 2) and the second is to occur in 2009 (Year5), and will be planned using results from the pilot experiment which took place in September 2008. A preliminary experiment was conducted in 2005 (Year 1) to aid in the design of the major field efforts. The research involves four main areas - (1) *in situ* measurements, (2) remote sensing, (3) modeling, and (4) physics and classification of coherent structures. The *in situ* field measurements are used to characterize the overall flow field to investigate the generation of coherent structures at specific sites, and initially, to provide boundary inputs for the numerical models. The surface signatures of coherent structures in the same region are detected using remote sensing techniques and compared with the *in situ* and model results. Results from the *in situ* field observations, remote sensing, and numerical model runs will be synthesized into a classification scheme that includes all observed coherent structures. Predictive scaling relationships will be developed in order to generalize the results from this study to other systems. The result of this integrated approach will be a thorough investigation of the mechanisms and evolution of coherent structures in rivers and estuaries in order to link their surface expressions to subsurface flow features.

The project participants have been organized into teams identified by the main areas of interest listed above: Remote Sensing: A. Jessup, C. Chickadel (APL-UW), W. Plant (APL-UW); Modeling: R. Street and O. Fringer (Stanford); In situ Measurements: S. Monismith and D. Fong (Stanford); Physics and Classification: A. Horner-Devine.

WORK COMPLETED IN FY08

The focus of this reporting period was:

- analysis of the data from the first major field experiment (2006)
- ongoing numerical modeling effort
- exploratory laboratory experiment
- pilot field experiment in preparation for 2nd major field experiment in 2009

This report will focus on the following areas:

- Thermal IR imaging (barge and airborne) (UW, APL)
- In Situ Measurements of Estuarine Dynamics (Stanford)
- Physics and Classification of Coherent Structures – lab expt. (UW, Civil and Env. Eng.)
- Numerical Modeling (Stanford)

- Microwave Remote Sensing (UW, APL)

RESULTS

THERMAL IR IMAGING

Analysis of thermal infrared (TIR) imagery continues with a focus on understanding the internal structure of riverine flow from surface signatures. We take a multi-layer approach to quantify and investigate riverine coherent structures from scales of individual boils (1cm - 5m) to river widths (10^2 m). The following steps were taken this year to achieve our larger goal:

1. Preliminary groundtruth and analysis of 1D infrared based particle image velocimetry (PIV)
2. Surface TIR measurements of scale laboratory unidirectional flow over a Gaussian bottom structure, and
3. Field TIR and *in situ* measurements of surface boil signatures, and large-scale flow in the Snohomish River.

Thermal Infrared PIV

A one-dimensional PIV technique was applied to IR measurements from the 2006 experiments. For computational speed and simplicity, the technique under investigation operates on frequency-wavenumber spectra of short video time series. We applied our frequency based PIV technique to this data with the goal of measuring the mean velocities and the magnitude of velocity fluctuations. Ground-truth comparisons were made with near-surface velocity measurements from a collocated acoustic doppler current profiler (ADCP). Figure 1 shows an example of the plan view of the 2006 TIR field of view, locations of the ADCP and PIV sample array, and a time series of PIV surface and *in situ* downstream velocity.

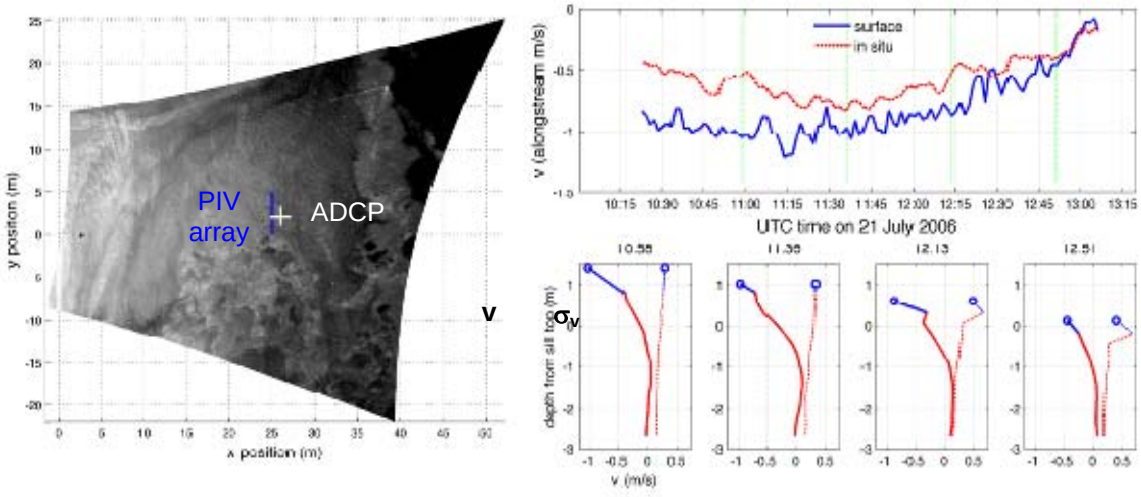

Figure 1. (left panel) Planview TIR image of flow over a sill (warmer=brighter) with PIV and ADCP locations indicated. (top right panel) Time series of surface PIV and near surface ADCP velocities during a falling tide. (bottom right panels) Combined profiles of the 3-min. mean (v, solid) and standard deviation (σ_v, dashed) velocities from PIV (blue) and ADCP (red).

Results demonstrate that surface TIR PIV compares well with the upper bins of the collocated ADCP and suggests a surface velocity shear. The near surface shear decreases as the flow slackens. Examples of the combined PIV and ADCP vertical profiles (Figure 1) suggest that there may be a subsurface velocity minimum in the ADCP due to breakdown of the signal coherence, but more rigorous testing is required to confirm this. An additional fortuitous discovery is that the velocity variability (3 min. standard deviation of velocity) measured from the ADCP and the surface PIV are nearly identical. This discovery will provide for augmented analysis of river or estuary flow turbulence through no-contact means and will be directly useful for measurement and analysis of river turbulence in future experiments.

The next step for TIR PIV development will be to extend our current 1D PIV technique to two-dimensions for measuring surface river circulation and for verifying our boil kinematics model. For demonstration, we have used our 1D technique to measure the alongstream surface velocity over the submerged sill (e.g. Figure 2). With surface flow maps like these we plan to investigate techniques for estimating the underlying bathymetry, and for guiding and testing hydrodynamic models. In addition, using 2D PIV mapping of fast-sampled, high-resolution TIR boil eruption imagery we will further test our working hypothesis that boils are shed from bottom features and advect upwards as horseshoe-shaped vortices through analysis of surface vorticity.

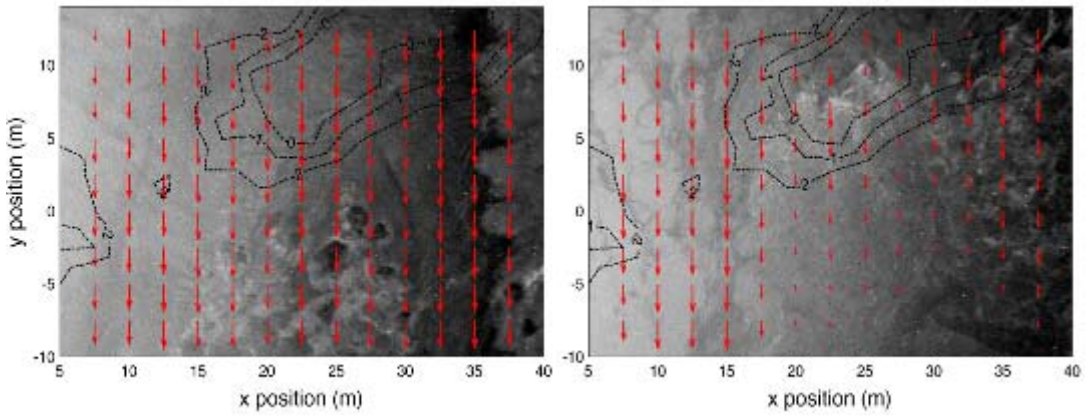

Figure 2. (left panel) Planview TIR snapshot, bathymetry and 1D PIV velocity estimates (max velocity shown ~1m/s) over the sill during max ebb. (right panel) Snapshot of alongstream flow ~1 hour later showing blocked flow downstream of the sill.

2008 Field Experiment

During the week of 15 September we deployed collocated TIR imagers and acoustic current meters to capture a range of scales of surface and interior flow measurements in the Snohomish River (Figure 3) downstream of a natural abrupt bottom feature. Two TIR imagers were deployed onboard the Henderson barge from towers (3m and 10m tall) to measure detailed surface temperature maps of boil scale processes (AIM fov ~3m, FLIR fov ~15m). Within the camera fields of view, two Nortek Aquadopp ADCPs and a Nortek Vector ADV were deployed to simultaneously measure interior and near-surface river flows. Full river width images (~100m) of the river were measured from the thermal imaging package deployed from the Helikite.

Preliminary data from the thermal infrared systems show that surface boil disruptions are ubiquitous on the river. At this location, ~15km upstream of the river mouth, tides modulate the river flow and boil activity with little or no salt wedge intrusion. Figure 4 shows thermal snapshots from the beginning and middle of ebb tide as the surface of the river becomes increasing disrupted by boil eruptions. Future analysis will include characterization of the developing boil field and surface velocity patterns in proximity to the bathymetry feature with changing conditions (tide level, flow speed). *In situ* velocity profiles will be used to groundtruth and understand surface thermal PIV velocity fields with the larger goal of quantifying the effect of bathymetry features and bottom roughness on observable surface river flow.

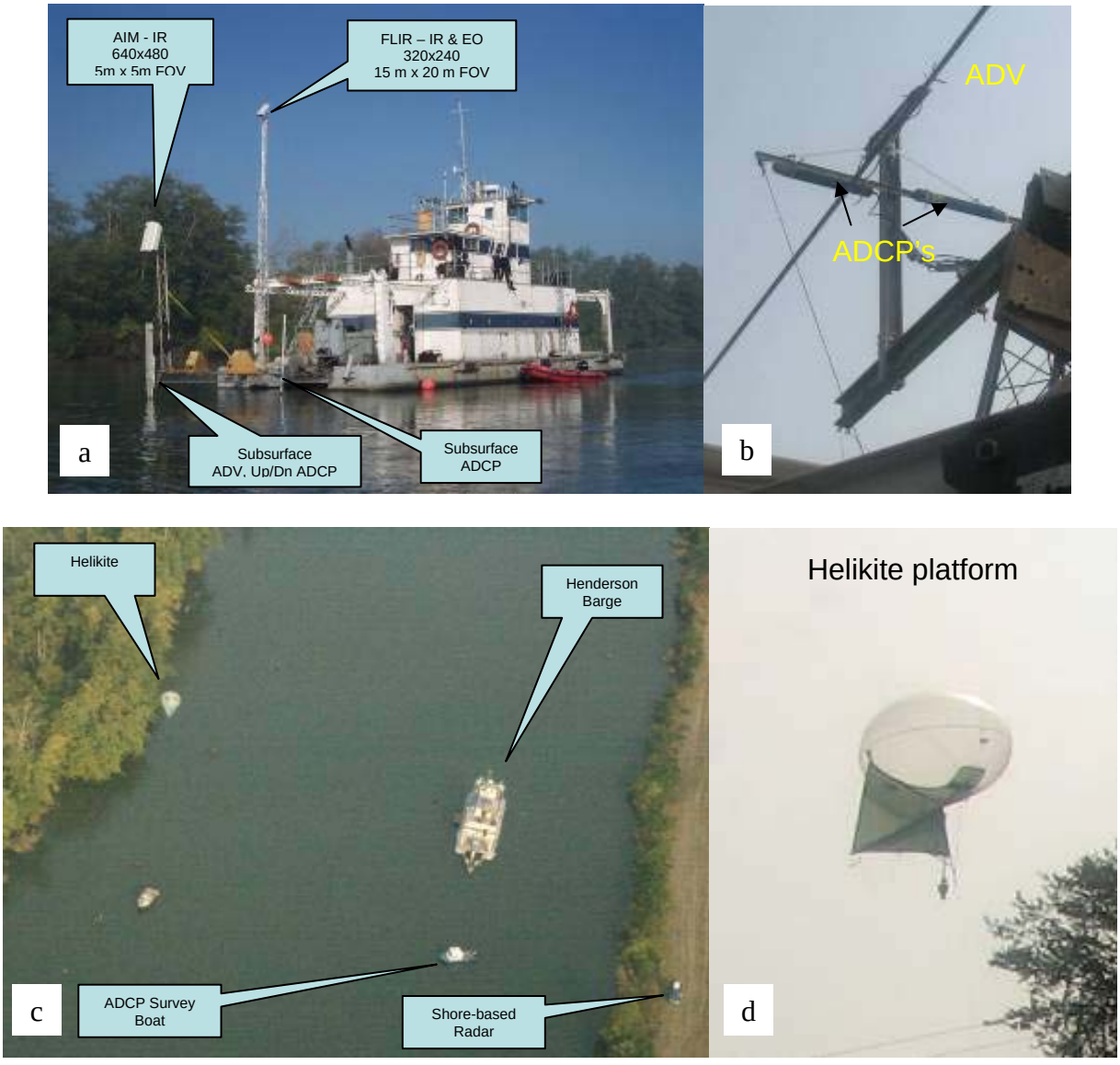

Figure 3. (a) Henderson barge showing configuration of the AIM and FLIR IR imagers with nested fields of view and location of current meters. (b) Two Aquadopp ADCP's and a Vector ADV were deployed from a submersible frame (shown in the raised position) to measure in situ river and boil velocities (c) Aerial photograph of measurement site showing relative locations of platforms (d) The Helikite thermal camera measured synoptic river imagery.

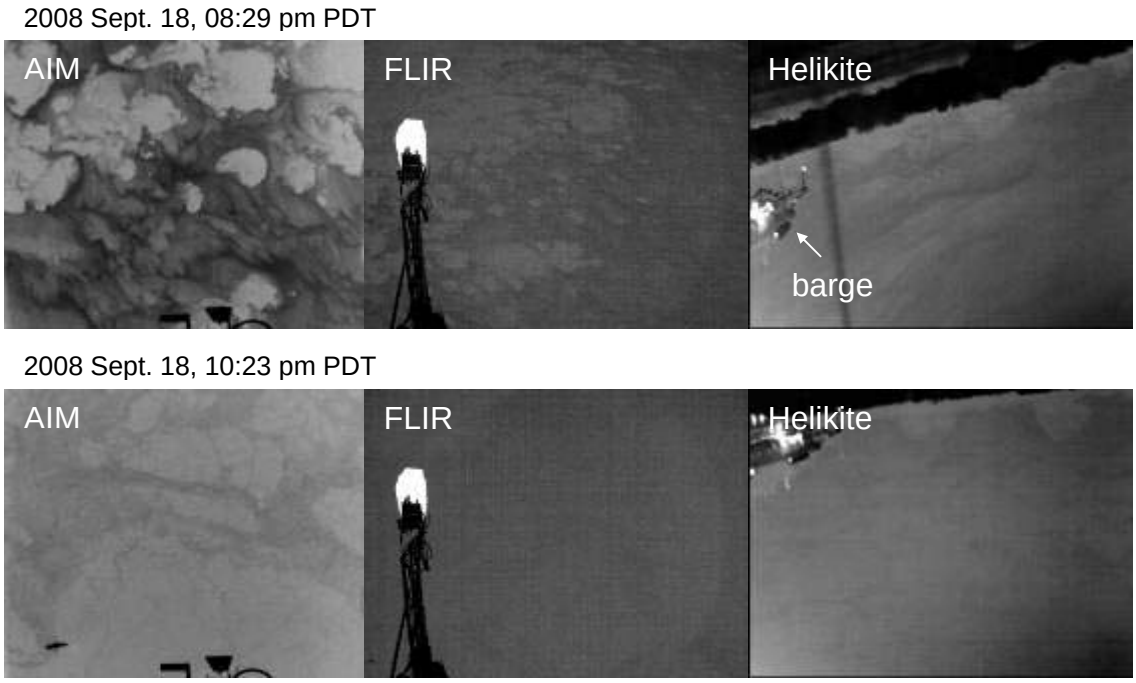

Figure 4. (top panel) TIR nested fields of view of ebb river flow showing the boil character near the beginning of the ebb. Note the strong contrast of the individual boils (bright) in the imagers. (bottom panel) Surface temperature ~2 hours later when the full river surface is disrupted and individual boils are not quite distinct.

IN-SITU FIELD MEASUREMENTS

During FY2008 the efforts of the in-situ team have been focused on further analysis of the data obtained in July 2006 as well as preparing for and conducting a pilot study in September 2008 to prepare for the 2009 field season. The work completed on the 2006 data has been presented at several conferences and are forming the basis for two papers currently in preparation. The September 2008 preliminary study provides us with important hydrodynamic information at the site.

Further analysis of July 2006 data

The active areas of research utilizing the 2006 dataset include further analysis of the shoal/channel induced frontogenesis that occurs at the tip of Jetty Island, general circulation and dispersion mechanisms in the Snohomish, and trying to understand tidally averaged parameters in a shallow, macrotidal estuarine system. A full explanation of the mechanism for frontogenesis and its effects on mixing and stratification as it develops has been completed and we are working on a manuscript comparing this with the infrared measurements and modeling results.

The second paper in progress describes the overall circulations and longitudinal dispersion in the Snohomish River Estuary. Detailed analysis of the longitudinal dispersion indicates less spring-neap variability than expected in the longitudinal dispersion coefficient, K_x and rather more subtidal variability. Tidal straining, complex bathymetry, and shoal/channel interactions contribute to more

complicated feedback mechanisms which alter the subtidal pattern of vertical mixing and dispersion and are being explored in great detail.

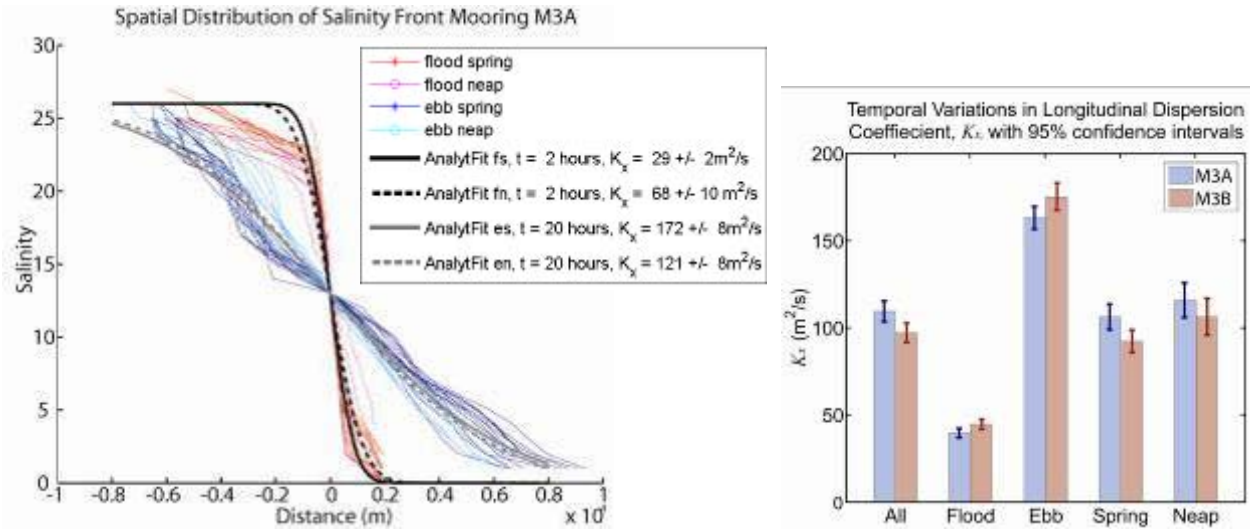

Figure 5. Longitudinal Dispersion Coefficient computations and results

The left panel of Figure 5 shows the salinity as a function of distance from the salt-wedge center. K_x is computed by fitting the data to the analytical solutions (thick grey and black lines). K_x varies temporally as shown in the bar chart on the right panel of Figure 5 for two July 2006 moorings.

Finally, due to the large tidal range and shallow depths of this estuary, this dataset is a wonderful tool for trying to better understand tidally averaged parameters in this type of system. These parameters are not well defined in estuaries of this nature and further analysis would provide a large contribution to the estuarine hydrodynamics community.

Snohomish September 2008 Pilot Experiment

During September 2008 we deployed one mooring and two transecting Acoustic Doppler Current Profilers (ADCPs) to provide the hydrodynamic conditions during the preliminary study in preparation for a larger experiment planned for summer 2009. Figure 6 shows the local bathymetry and the locations of the barge, mooring, and transect paths. The mooring was located upstream, south, of the barge and had a bottom mounted ADCP and CTD (Conductivity, Temperature, Depth sensor) as well as a CTD at the water surface. The mooring was leveled by divers in order to also obtain measurements of turbulent Reynolds stresses. In addition to the mooring, we had one fixed ADCP mounted on the barge looking downwards in the field of view of the camera. The goal of this ADCP was to determine if it is possible to obtain turbulent Reynolds stresses from this platform and to measure the currents in the immediate vicinity of the other instruments. Finally, we established four transect paths to repeat ADCP transecting during both flood and ebb tides as marked in Figure 6 . In addition to these transects, we completed a detailed bathymetric survey.

The left panel in Figure 6 marks the region of study in the Snohomish River Estuary shown in greater detail on the right map. Contours are meters below a -1m tide and the Henderson Barge platform location, mooring location, and transects are marked.

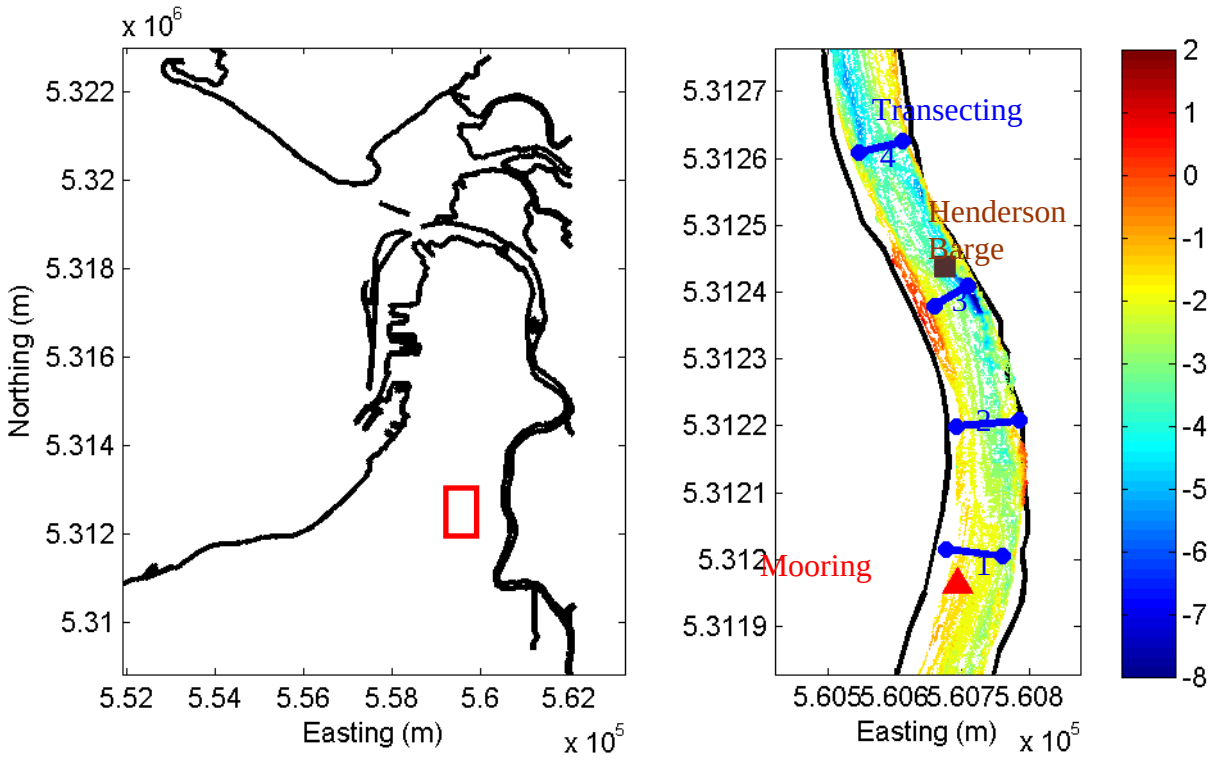

Figure 6 Snohomish September 2008 Preliminary Study Region

Figure 7 shows the along channel and cross channel velocities at the mooring derived via principal component analysis as well as the density computed from the top and bottom CTDs. The velocity shows a strong tidal influence as we expected with currents exceeding 1.3m/s. The cross channel velocities exhibit secondary circulation in the sense expected due to the local river curvature (towards the outer bank at the surface and towards the inner bank at the bottom). The system behaves largely as a well mixed estuary; however, there is vertical stratification (up to 3 kgm^{-3} in almost 5m of water ~ 0.6 kgm^{-4}) during the stronger spring tides. This stratification does play a role in the physics as evidenced in the cross channel velocities and strong lateral convergences we observed in the region.

The top two graphs in Figure 7 display the along channel (top panel) and across channel (mid panel) velocity from the moored ADCP derived via principal component analyses. Positive along channel flows are in the direction of the flooding current (approximately towards the South) and positive cross channel flows are towards the outer bank (Eastern bank) of the river. The bottom panel plots the top and bottom density derived from the moored CTDs. Blue boxes mark transecting times and the red line indicates the time of the transect displayed in Figure 8 .

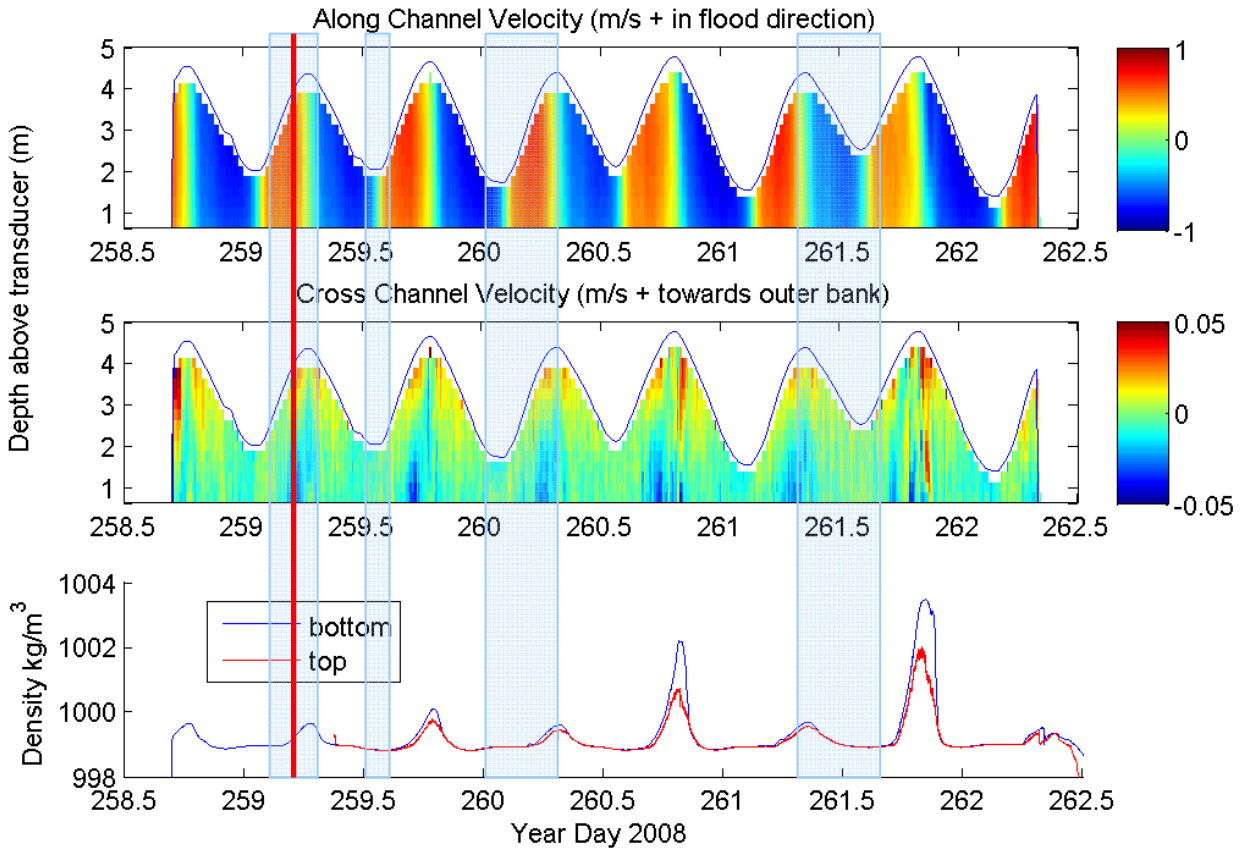

Figure 7 Snohomish 2008 Preliminary Study Mooring velocity and stratification

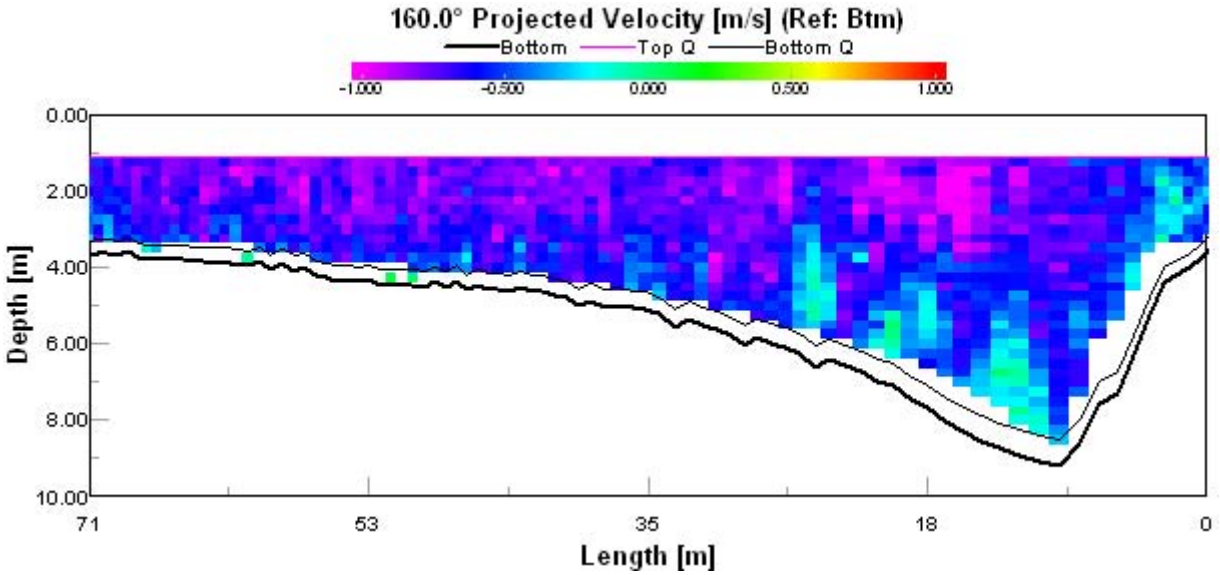

Figure 8. Along channel velocity from ADCP transect 3, near the barge field of view. The length along the x axis indicates the distance from the Eastern edge of the transect. Velocity is negative in the direction of the ebb current (~NW).

Figure 8 shows one ADCP transect near the barge field of view during peak ebb currents when boils can be observed. The time of this transect is marked in a red line on Figure 7 . In the bathymetric depression there is strong vertical shear in the currents corresponding with a region of different backscatter (not shown here). Further analysis of this data set in conjunction with the infrared images may lead to a better understanding of boil signatures and boil generation.

The ADCP aboard the barge has not yet been fully analyzed. A first look at the data seems to indicate that we can certainly obtain mean currents from this instrument but that we may not be able to get turbulent stresses due to contamination from the barge movement. However, this needs further time to confirm and we will be working with the UW in-situ team to further analyze this data.

The depth survey has not yet been corrected for the tidal elevation so cannot yet be compared to the previous data. However, once processed this data will be useful in determining whether the bathymetry changes on a seasonal time scale due to flow events. The other potentially interesting data we can use to look at bed changes will be the data from the ADCP fixed on the barge. It may be possible to examine the bottom track data on that instrument to back out local bed motion as long as we can adjust well for the barge movements. These are both areas we plan to research in more depth as we work more with this data set.

Overall, this preliminary deployment was a success from the point of view of the in-situ instrumentation. We are confident that we can do a successful job of deploying moorings and boat-mounted instrumentation again in 2009 that will aid the other members of the COHSTREX team. We can provide both the background hydrodynamic conditions and more detailed measurements that may aid in understanding boil generation and evolution. The only aspect that may not be as promising as hoped is the ability to obtain turbulent stresses from the ADCP fixed aboard the barge, however, we plan to explore that more fully in the coming months.

PHYSICS AND CLASSIFICATION OF COHERENT STRUCTURES

Work on the physics and classification of coherent structures has been focused in three areas:

(1) Analysis of the dynamics of flow over a rocky sill in the Snohomish river estuary using data from the 2006 field experiment. Our primary conclusion is that flow separation, followed by the growth of a mixing layer downstream of the sill, controls the development of coherent structures and surface boils at this location.

(2) Laboratory experiments investigating the dynamics of flow over an idealized, 2D sill. Boils generated from the sill were imaged in the water column using dye and as they impinged on the water surface using infrared imaging. These results confirm that mixing layer dynamics control the surface expression of boils, and point to the importance of flow depth (and to a lesser extent, flow velocity) on the frequency and location of boils.

(3) In September 2008 we executed a week-long pilot experiment on the Snohomish river to help plan for the 2nd major field experiment in 2009

Echosounder Measurements: In-situ Dynamics

We characterized the mixing/shear layer observed during ebb tides in the lee of a rocky sill using a combination of velocity and Biosonics echosounder data (Fig. 9 and Fig. 10). Flow separation occurs on the sill, causing recirculation beneath the near-surface outflow (Fig. 9a). The near-bed, upstream flow is entrained upwards into a mixing layer (Fig. 9b), which is characterized by a strong horizontal and vertical velocity gradient (Fig. 10). The boundary between the recirculation 'bubble' and the downstream flow varies over time. Early in the ebb tide, an internal lee wave forces the boundary downwards (see Fig. 9a, 9b, and 9d). As stratification disappears (Fig. 9c), the boundary rebounds, only to decrease again as water level falls and the surface boundary exerts constraints on the mixing layer (Fig. 9a, 9d). This behavior is typical of the greater ebb during all days of the July 2006 experiment. Over smaller, 6 minute time snapshots (Fig. 10), both vertical and down-stream flow show an inflection point that denotes the mixing layer boundary and coincides with the increased echo return in the upper layer. The echo-return hence delineates a boundary in mixing; close inspection shows that this boundary fluctuates with the internal mixing dynamics, which are imaged as a series of high-return diagonals stitched together to form a helical pattern. Strouhal scaling and spectral analysis suggest that the high-return diagonals are formed by vortices in the mixing layer, while lower frequency variation (see lower layer boundary) is caused by the so-called flapping frequency of the recirculation bubble. The vortex frequency and flapping frequency are evident in surface IR measurements of boils (not shown), suggesting that the mixing layer/recirculation dynamics control the surface expression of coherent structures at this location.

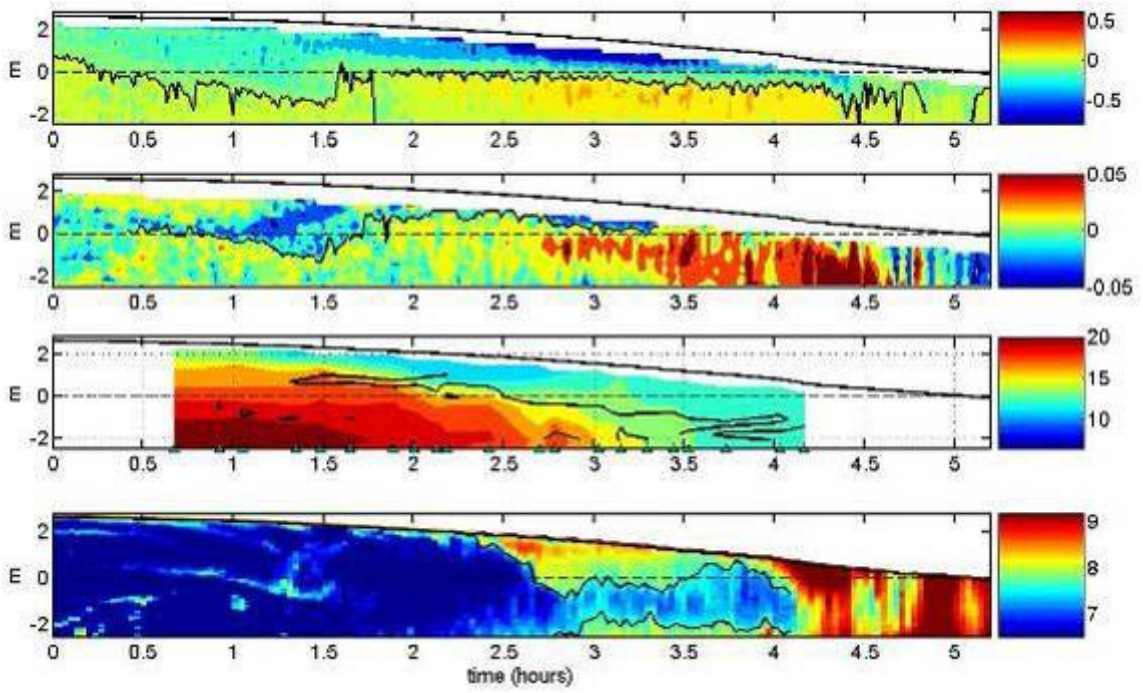

Fig 9. Horizontal velocity (a), vertical velocity (b), density anomaly (c), and Biosonics echosounder (d) during the greater ebb on July 21st, 2006. Time measured after HW.

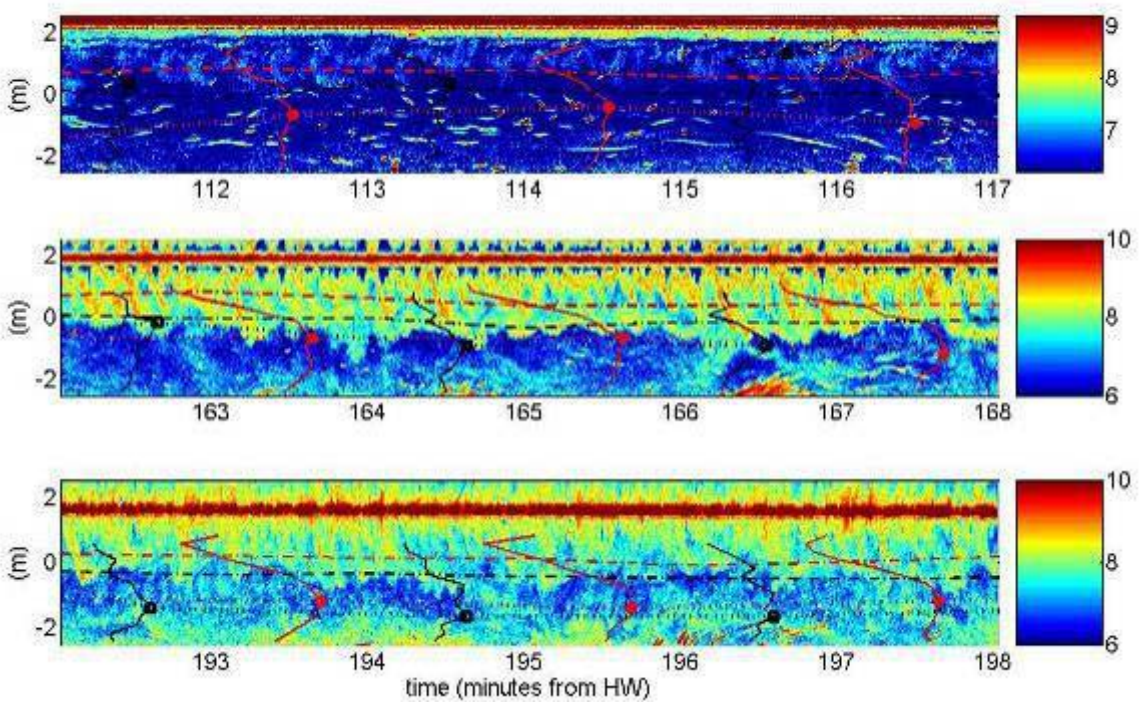

Fig. 10. Biosonics echosounder, overlaid with horizontal velocity profiles (red) and vertical velocity profiles (black) during three 6 minute snapshots during the ebb of July 21st, 2006.

Laboratory Experiments

In March 2008 we conducted a pilot laboratory experiment to measure *in situ* flow and surface TIR signatures. We gathered data on boil development, recirculation and internal coherent structures due to the abrupt bathymetry element by operating the flume at varying flow depths and fluid speeds over a modeled "sill". These measurements were designed to inform us about recent and upcoming field experiments in the upper Snohomish River. In particular, the mechanism for visualizing boils in the laboratory relied on heating the flume water to induce a net outward heat flux resulting in a cool skin layer. Boils were revealed as disruptions in the cool skin by upwelling of warm underlying water. In the same way the net outward heat flux in the Snohomish River allowed visualization of boils erupting there (see examples below).

Laboratory measurements of coherent structures over a sill (see Fig. 11) are consistent with our evolving picture of boiling activity in the Snohomish sill, and show that vortex structures caused by the sill impinge on the water surface as boils. A dye release (Fig. 11a and Fig 11c) shows the spatial development of instabilities caused by shear between free-stream flow and the recirculating flow (Fig. 11e). These instabilities 'roll up' to create vortices, then grow as they combine with each other downstream (Fig. 11a and Fig. 11c). Surface boils (seen as red, warm circular patches in the IR signal) clearly occur when sill-sourced vortices impinge the surface (Fig. 11b and Fig. 11c). The mean location of boil surfacing corresponds to the location that the mixing layer (characterized by elevated turbulent kinetic energy, TKE) surfaces and surface flow decelerates (Fig. 11e and Fig. 11f); as depth increases, both the mixing layer and boils surface further downstream (Fig 11d). These results

confirm the importance of the shear/mixing layer to the development of subsurface instabilities, vortices, and ultimately surface boils. Future lab experiments would be a good way to increase our understanding of boils.

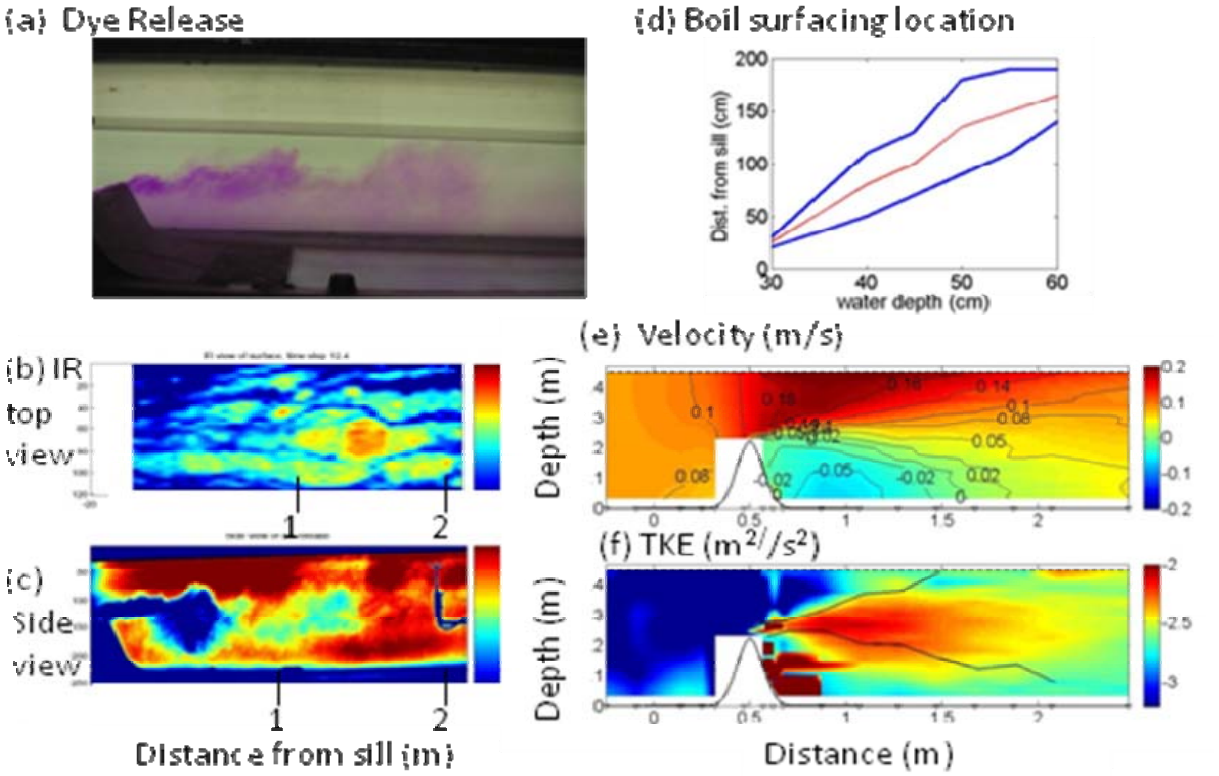

Figure 11: Snapshots of (a) dye release at sill crest of laboratory study, (b) top view of flume using an IR camera, (c) simultaneous side view of die release in (b) using video camera, (d) envelope of boil surfacing as a function of water depth and distance from sill, (e) average horizontal velocity, and (f) average vertical velocity. Flow is from left to right; in the side view plots, the 22.5 cm sill is seen in the bottom left corner. Water depth was 45 cm, and mean flow ~ 9 cm/s.

Snohomish Pilot Project

From September 15th to September 19th, 2008, an array of Biosonics echosounders on the Snohomish River was tested as part of the 2008 pilot project. Three transducers with a frequency of 1000 kHz, 420 kHz, and 200 kHz were tested in several different configurations, including forward looking (into the flow), downward looking (towards the bed), and combined (both forward and downward looking). The goal of the experiment was (a) to determine if the instruments can image coherent structures in a riverine (not estuarine) environment and (b) to determine the differences in imaging between the different acoustic frequencies. Results are currently being assessed.

NUMERICAL MODELING

Estuary-scale simulations with SUNTANS

During the past year we have focused on understanding the influence of aspects of high-resolution estuarine modeling that affect the results in our SUNTANS simulations, namely the bathymetry, specification of bottom stress, computation of the nonhydrostatic pressure, accurate advection of momentum, and fresh water inflow. These results are presented in detail in a paper published in a special issue on unstructured grids in Ocean Modelling (Wang et al., 2008). Here we summarize the key points in that paper relating to bathymetry and computation of the nonhydrostatic pressure. Our most significant finding was that high-resolution simulations require high resolution bathymetry. Although numerous bathymetric surveys were performed, it was not until the survey of Chickadel et al. (2008) that we were able to obtain satisfactory agreement between measurements and the simulations. Figure 12 shows that, prior to obtaining the bathymetry to the north of Jetty Island, the mudflats were much deeper using the coarse data set of Finlayson (2005). The updated bathymetry enabled accurate wetting and drying of the mudflats and thereby accurate simulation of the flow through the bypass channel (which is to the left of the A-A' transect in Figure 12b).

When high resolution is employed, it also becomes necessary to compute the nonhydrostatic pressure. In an effort to assess the nonhydrostatic effects in our simulations, we compared the results of SUNTANS with and without the nonhydrostatic pressure. While the tidal dynamics are largely hydrostatic, since the ratio of the vertical to horizontal length scale of this flow is very low, flows around complex topography can be strongly nonhydrostatic. Figure 13 depicts the transverse flow parallel to transect A-A' (see Figure 12) computed by the nonhydrostatic simulation at four different stages of the tide, namely (a) early ebb, (b) late ebb, (c) early flood, and (d) late flood. The contours indicate the difference between the nonhydrostatic and hydrostatic simulations, and show that regions of short horizontal variability appear in the flow both at and away from boundaries at all stages of the tide. These regions are strongly nonhydrostatic and indicate that nonhydrostatic effects cannot always be estimated based on channel geometry, since the ratio of the depth to the width of this channel is quite small (0.01). Instead, it is more appropriate to estimate nonhydrostatic effects based on the flow length scales. Here, the horizontal length scale of the contours that represent a departure from hydrostacy are much smaller than the width because they are induced by flows not directly tied to the local bathymetry. In particular, the contours in the upper-middle portion of the water column in Figure 13(c) represent the confluence of the river and mudflat flows which is observable using remote sensing imagery (both IR and Radar). This confluence consists of two counter-rotating vortices that are strongly nonhydrostatic.

Idealized channel simulations with PCUI

We have performed simulations with the parallel, curvilinear-grid, large-eddy simulation code known as PCUI (Cui and Street, 2001;2004) to help understand how surface signatures are correlated with bottom bedforms in an idealized channel flow geometry with a rigid lid. The bedforms studied are shown in Figure 14, and these have amplitudes varying from 0.1D to 0.4D, where D=2.5 m is the undisturbed depth of the domain. With periodic boundary conditions in the lateral and a quadratic drag law formulation on the bed, a constant pressure gradient is imposed that accelerates a mean streamwise flow to roughly 0.5 m s^{-1}. We find that the turbulent flowfield associated with the boundary layer in the flow in the absence of bottom bedforms (Figure 15 depicts the flow around a Gaussian hill) overwhelms the surface signatures, thereby rendering it almost impossible to distinguish among the

different bedforms based on instantaneous properties of the flow, such as the vertical velocity (or horizontal divergence) just below the lid, as shown in Figure 16. Although time-averaged properties are highly correlated with the bedforms, such as the pressure distribution below the lid as shown in Figure 17, the pressure signal is not detectable by even the most sensitive instrumentation. We find that, contrary to our initial hypothesis, turbulent properties of the flow actually degrade the correlation of the bedforms with the free surface signatures. Rather, the highest possible correlations exist under steady, irrotational flow conditions. This is exhibited by a time-history of a typical correlation of surface flow features with bedforms, which shows that initially the correlation is high, but the correlation decreases upon flow separation and the transition to turbulence.

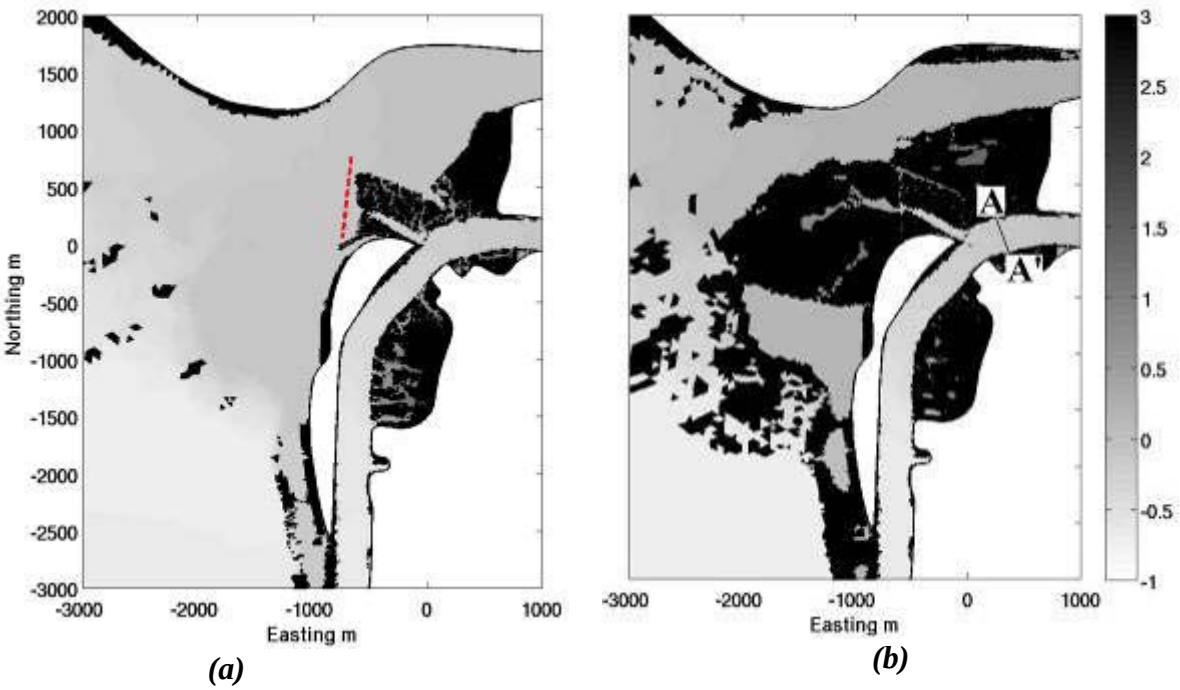

Figure 12: Intertidal mudflats exposed during LLW on (a) the old bathymetry and (b) the new bathymetry. Grayscale shading indicates free-surface height in m above MLLW, and the dashed line in (a) indicates where the old survey data ends. Data along transect A-A' is presented in Figure 13.

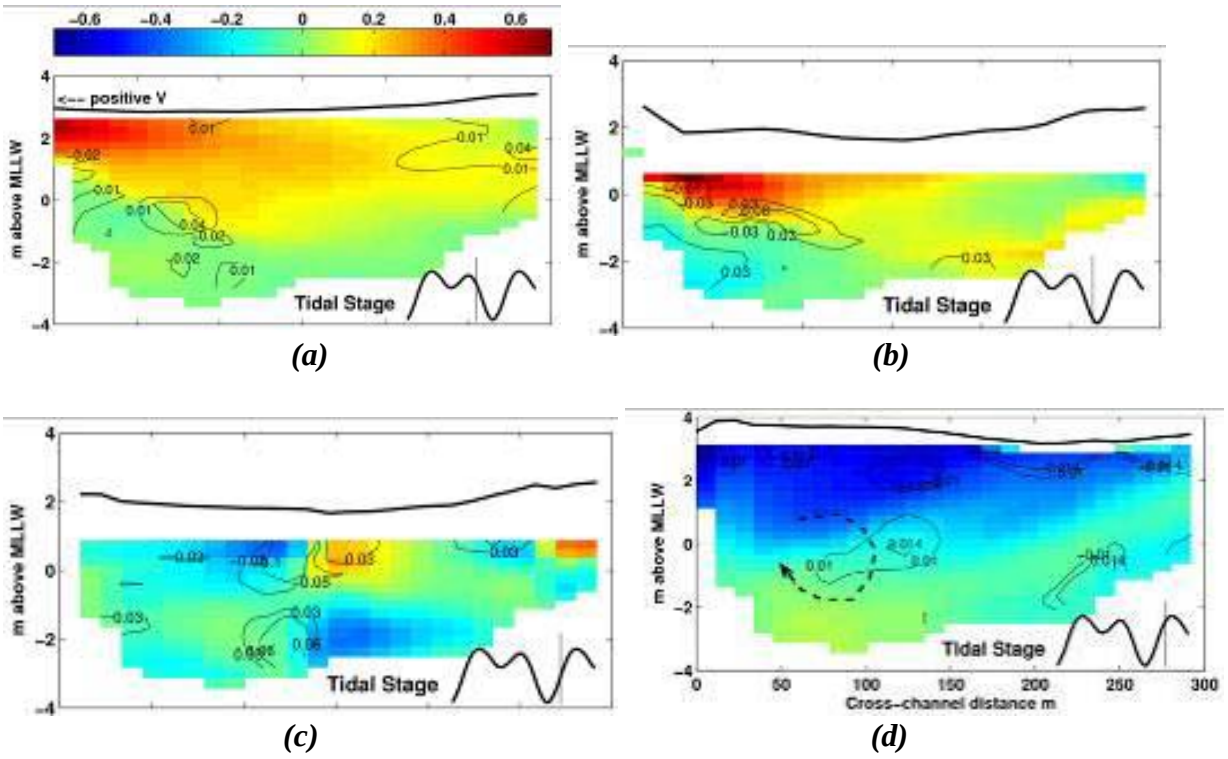

Figure 13: Transverse velocity profiles (m s^{-1}) at transect A-A' (see Figure 1) during early ebb (a), late ebb (b), early flood (c), and late flood tide (d). Contours depict differences between the nonhydrostatic and hydrostatic simulations, while the transverse velocity is positive to the left in the figure. The dashed arrow indicates a region of flow separation over the left bank.

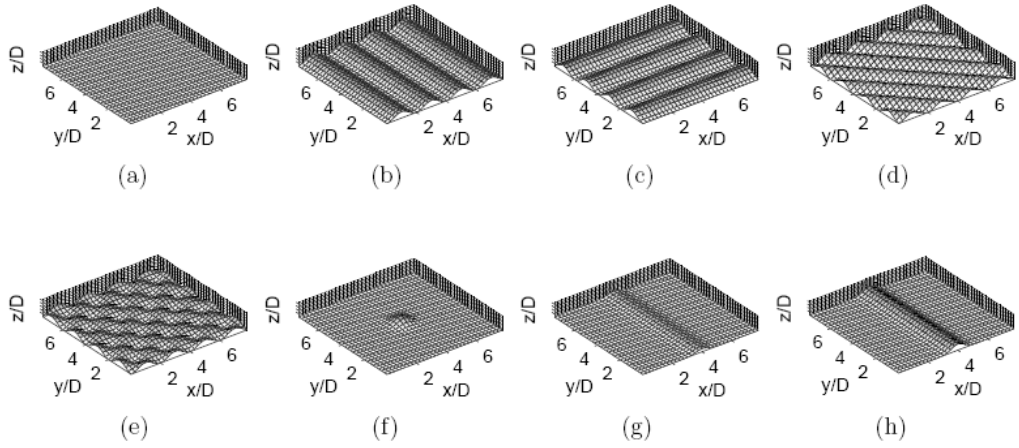

Figure 14: Bedforms investigated in the bedform study: (a) flat, (b) lateral, (c) longitudinal, (d) diagonal, (e) mixed, (f) 3D Gaussian, (g) short 2D Gaussian sill, and (h) tall 2D Gaussian sill. Mean flow is from lower left to upper right.

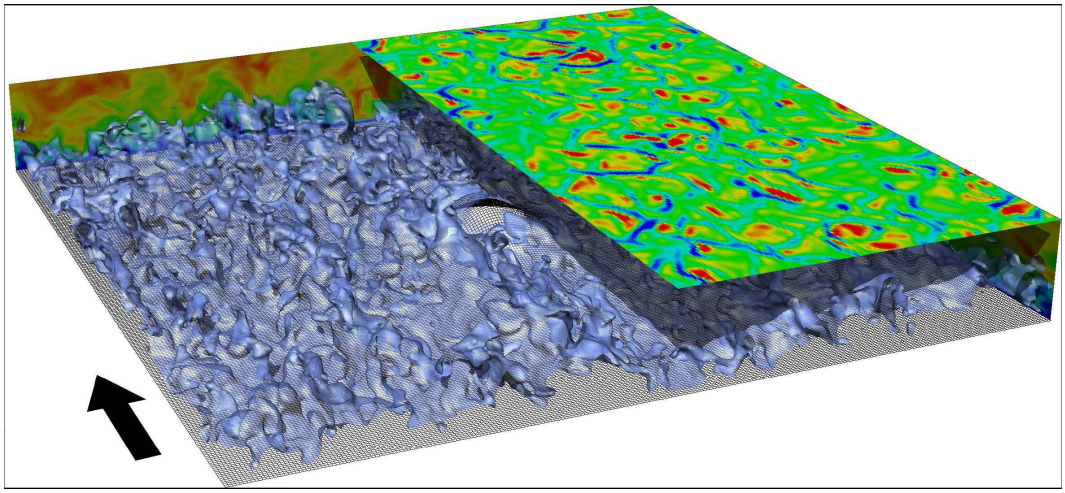

Figure 15: Visualization of flow past a centered 3D Gaussian bump. Isosurfaces are of u/U =1, where U=0.5 m s^{-1}, vertical wall slices are colored by the streamwise velocity, and the clipped horizontal pseudocolor plot is of the vertical velocity for the grid cell closest to the surface (red is upwelling, blue downwelling). Mean flow is from bottom right to upper left, parallel to the x-axis, as indicated by the arrow.

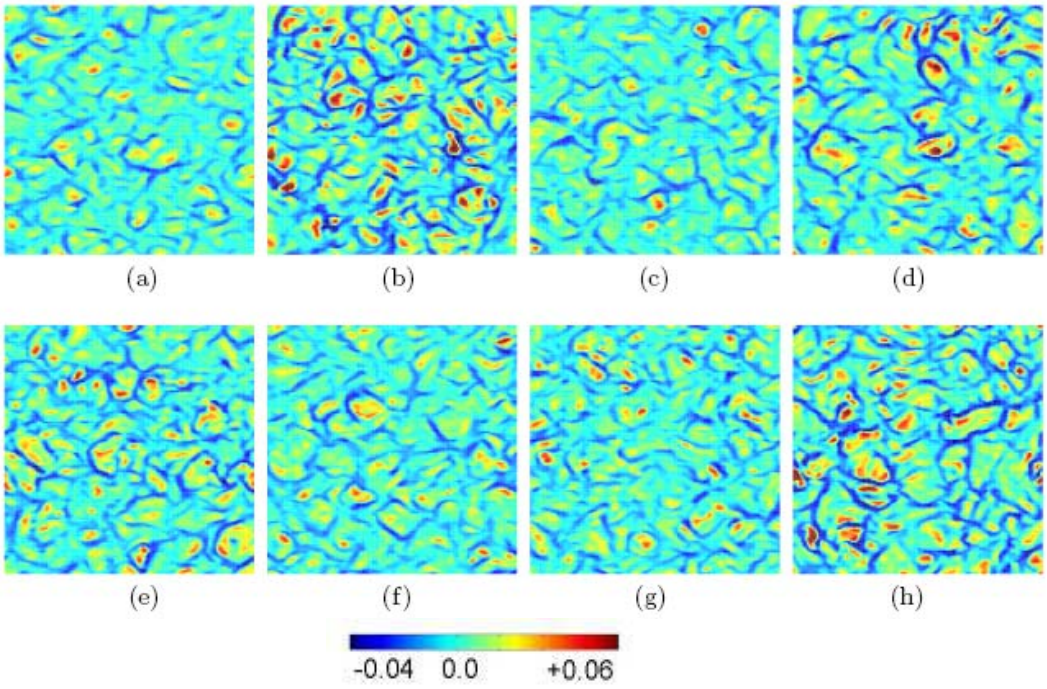

Figure 16: Instantaneous vertical velocity distribution (m s^{-1}) just below the lid for the bedforms depicted in Figure 3 after 22 flow-through periods. Mean flow is from left to right.

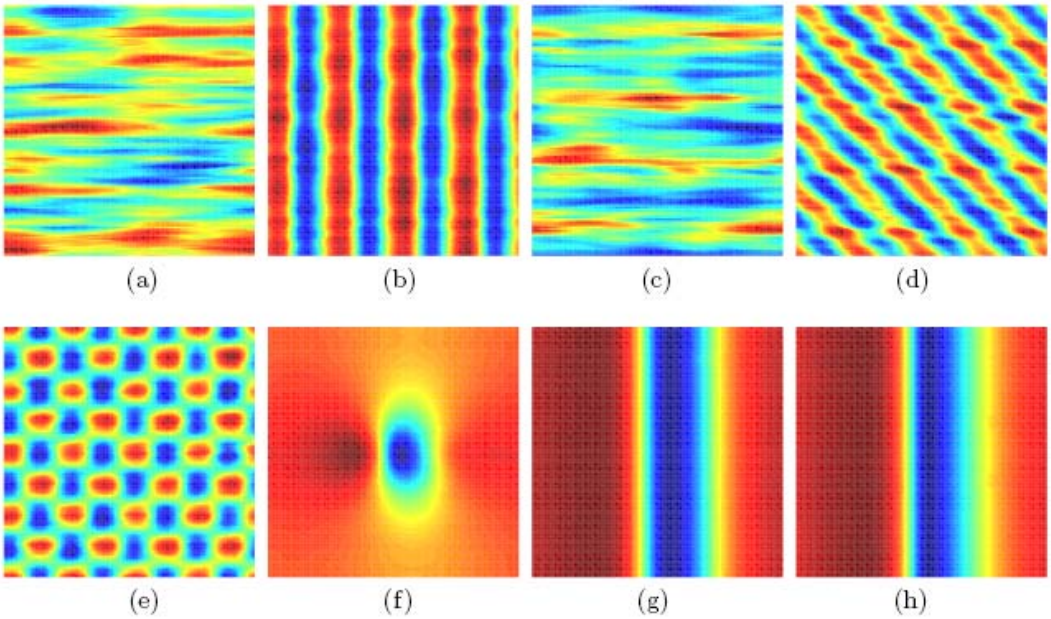

Figure 17: Time-averaged pressure just below the free surface for the bedforms depicted in Figure 14. Mean flow is from left to right.

MICROWAVE REMOTE SENSING

During the last fiscal year, we have continued the analysis of our ground-based microwave data collected by RiverRad on the Snohomish River near Jetty Island and have participated in two pilot field experiments farther upstream on the river, east of the city of Everett. We have written a draft paper of our Jetty Island results and are now working with our Stanford colleagues to compare these results with model output. The two field experiments included measurements using the ground-based RiverRad from a location on the dike east of the river as well as four days of flights on a Cessna Sky Hawk operating the microSAR that we borrowed from Brigham Young University.

In the draft paper "River Surface Features in Microwave Doppler Radar Images", we report on the complete set of RiverRad measurements made around Jetty Island. Here we report only two of the most important results from those measurements. The first of these relates to the frontal feature observed on flood tide at the convergence of water returning from the bypass and water in the main channel. Because of the nearly continuous nature of the RiverRad measurements, we were able to follow the movement of this front as the tide progressed toward high tide. Figure 18 shows the observed positions of the front at various phases of the tide. The west end of the front begins near the tip of Jetty Island when it is first observable midway between low and high tides. As time progresses and the tide moves toward its maximum, the west end of the front detachs from Jetty Island and moves south. This is followed at later times by the east end of the visible part of the front also moving south. This is the behavior observed in 2007. In 2005, the front did not detach from Jetty Island but remained stationary through the tidal phase just before high tide. It is this variable behavior that the Stanford group is now trying to model.

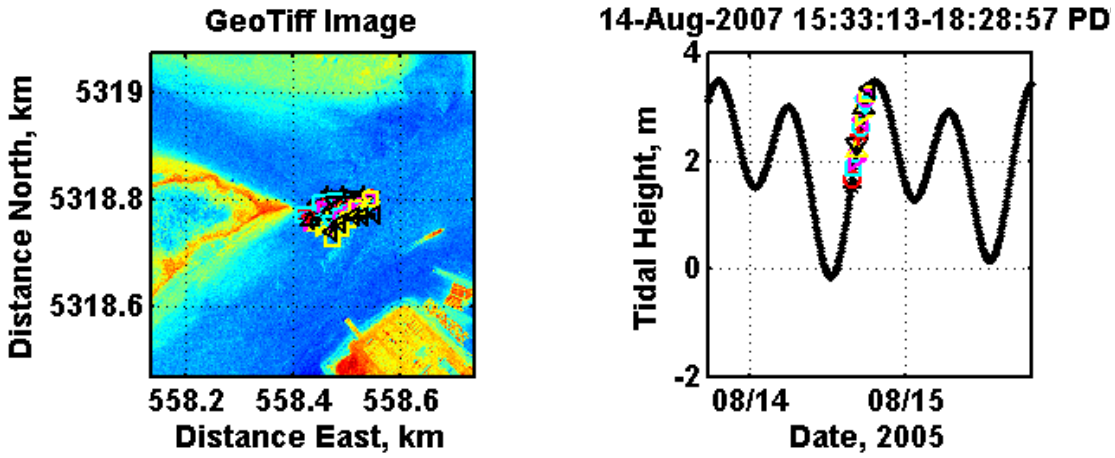

Figure 18. Location of the front observed by RiverRad in 2007. Times of the observations are shown on the right.

Another persistent feature observed by RiverRad near Jetty Island was a set of parallel bright (high cross section) lines just southeast of the tip of the sill, which is itself to the southeast of the tip of Jetty Island. The mystery of the source of these parallel lines has now been solved: they are due to flow over the deep hole that exists just south of the tip of the sill. Figure 19 shows the collocation of these lines with the edges of this hole. The Stanford group has been adding higher resolution bathymetry to their SUNTANS model near the sill in an attempt to explain the occurrence of these lines. They are almost certainly caused by gradients in the surface current set up by flow over the hole.

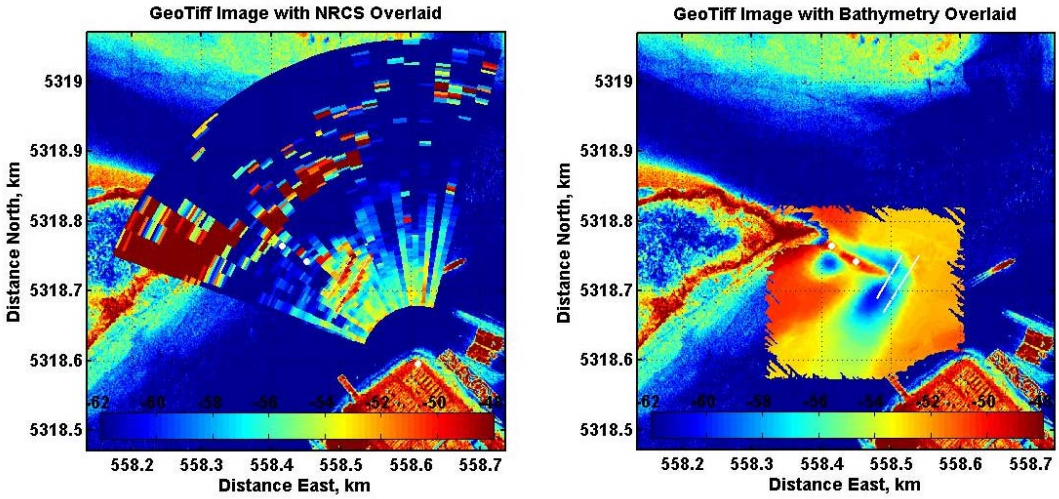

Figure 19. Coincidence between the image features observed near low tide and the sides of the hole in the bottom south of the tip of the sill. The white lines in the right image are at the locations of the bright features in the left image.

Data from our two pilot experiments, one in June 2008 and the other in September, farther upstream on the Snohomish River have not been analyzed in nearly as much detail as the earlier data. Figure 20 shows the equipment we operated during these two experiments.

Figure 20. Microwave equipment operated during two pilot experiments on the Snohomish River east of Everett in 2008. Left: RiverRad on an APL pickup. Right: the BYU microSAR on the Cessna Sky Hawk.

Data from the airborne microSAR have not yet been converted into images but RiverRad data from the first of the two experiments have been analyzed to show the river currents at different tidal periods. These are shown Figures 21 and 22. Clearly the influence of the tide reaches up the river to the point of our measurements as shown by the near cessation of flow at high tide. Flow on the west side of the river is always very low due to a number of pilings along that side.

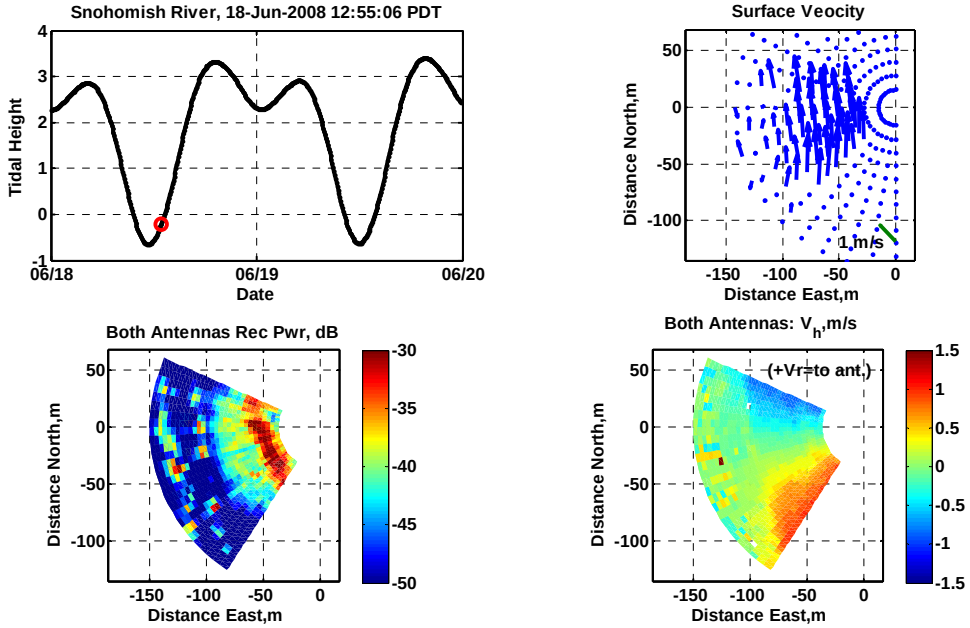

Figure 21. RiverRad data on the Snohomish River east of Everett just after low tide.

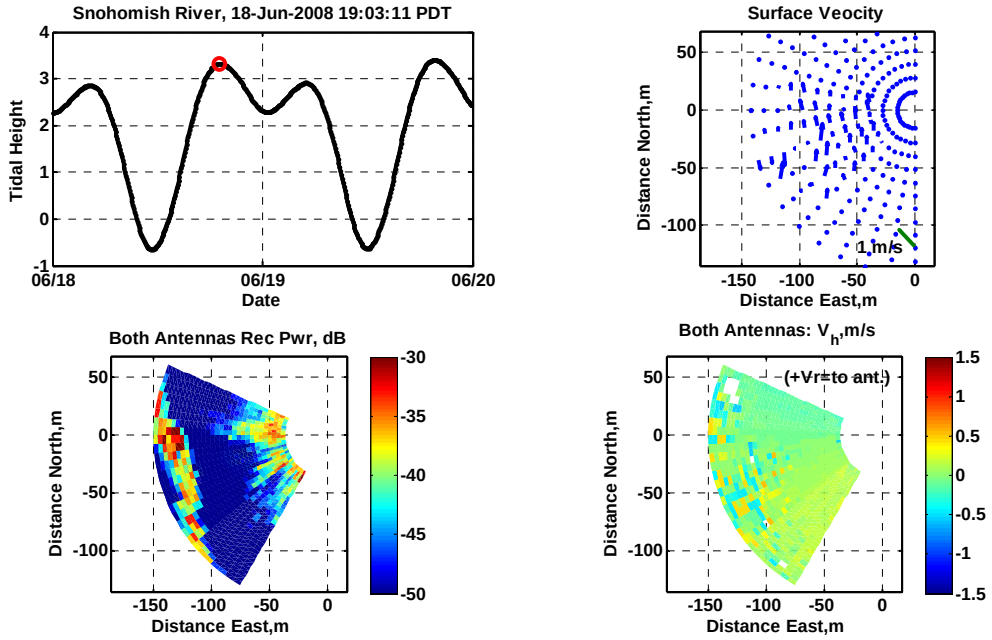

Figure 22. RiverRad data on the Snohomish River east of Everett at high tide.

IMPACT/APPLICATIONS

Our results demonstrate how currently available prediction schemes and observing systems (remote sensing and AUVs) can be combined for operational applications.

RELATED PROJECTS

Airborne IR/EO measurement system used for COHSTREX 08 Pilot Experiment was developed for Tidal Flats DRI.

REFERENCES

Chickadel, C.C., Horner-Devine, A.R., and A.T. Jessup, 2008, Thermal remote sensing of boils generated at a submerged estuarine sill. AGU Ocean Sciences Meeting, Orlando.

Cui, A., and R. L. Street, 2001, Large-eddy simulation of turbulent rotating convective flow development. J. Fluid Mech., 447:53–84.

Cui, A., and R. L. Street, 2004, Large-eddy simulation of coastal upwelling flow. Environmental Fluid Mechanics, 4:197–223.

Finlayson, D.P., 2005, Combined bathymetry and topography of the Puget Lowland, Washington State, www.ocean.washington.edu/data/pugetsound.

Wang, B., Fringer, O.B., Giddings, S.N., and D.A. Fong, 2008, High-resolution simulations of a macrotidal estuary using SUNTANS, Ocean Modeling, in press, doi:10.1016/j.ocemod.2008.08.006

PUBLICATIONS

Barad, M. F., and O. B. Fringer, 2007, Numerical simulations of shear instabilities in open-ocean internal gravity waves, Proceedings of the fifth internatioal symposium on environmental hydraulics.

Wang, B., Fringer, O.B., Giddings, S.N., and D.A. Fong, 2008, High-resolution simulations of a macrotidal estuary using SUNTANS, Ocean Modeling, in press, doi:10.1016/j.ocemod.2008.08.006

Wang, B., and O. B. Fringer, 2007, "Modeling the dynamics of the Snohomish River Estuary with a finite volume, unstructured-grid parallel coastal ocean simulator", *Proceedings of the fifth international symposium on environmental hydraulics*.